Supporting Information

Amino-Bridged Quantum Dots/Covalent Organic Frameworks S-Scheme Heterojunction for Photocatalytic Overall Water Splitting

Weiqiang Guo [a, b, e, ‡], Hongtao Li [a, b, e, ‡], Yan-Xi Tan[f], Lei Jiao [b, c, *], Zhendong Wang [b, e], Qian Feng [a, b, e], Xiang Zhang [b, c *], and Yaobing Wang[b, c, d, *]

[a]College of Chemistry, Institute of Molecular Engineering Plus, Fuzhou University, Fuzhou 350116, P. R. China

[b]CAS Key Laboratory of Design and Assembly of Functional Nanostructures, and Fujian Provincial Key Laboratory of Nanomaterials, State Key Laboratory of Structural Chemistry, Fujian Institute of Research on the Structure of Matter, Chinese Academy of Sciences, fuzhou 350002, fujian, P. RChina.

[c]Fujian Science and Technology Innovation Laboratory for Optoelectronic Information of China, Fuzhou 350108, Fujian, P. R. China.

[d]University of Chinese Academy of Sciences, Beijing 100049, P. R. China.

[e]Fujian College, University of Chinese Academy of Sciences, Fuzhou 350002, P. R. China

[f]Guangxi Key Laboratory of Chemistry and Engineering of Forest Products Guangxi Minzu University, Nanning, Guangxi 530006, P. R. China

*Corresponding authors.

‡ These authors contributed equally to this work.

Experimental details

Materials and Chemicals

The chemicals 1,3,5-triformylphloroglucinol (TPG), 3,3'-dinitrobenzidine (DNB), and tin(II) chloride dihydrate ($SnCl_2 \cdot 2H_2O$) were purchased from Admas, while cadmium chloride ($CdCl_2$), 3-mercaptopropionic acid (3-MPA), and sodium sulfide nonahydrate ($Na_2S \cdot 9H_2O$) were supplied by Sinopharm Chemical Reagent Co., Ltd. (Shanghai, China). All reagents were used as received without further purification.

Synthesis of NO_2-COF and NH_2-COF.

NO_2-COF was synthesized via a modified solvothermal method [1]. Briefly, TPG (0.25 mmol) and DNB (0.38 mmol) were combined in a mixed solvent of n-butanol and 1,2-dichlorobenzene (10 mL, 1:1 by volume). To this mixture, 1 mL of 6 M acetic acid was introduced as a catalyst. After transferring the solution to a Schlenk tube and sonicating for 10-15 min to ensure homogeneity, the tube was flash-frozen in a liquid nitrogen bath (77 K) and subjected to three freeze-pump-thaw cycles for degassing. The sealed tube was then heated at 120 °C for 72 hours. The resulting precipitate was isolated by suction filtration, thoroughly washed with ethanol, anhydrous DMF, and acetone, and finally dried under vacuum at 60 °C for 12 h, ultimately yielding NO_2-COF with an isolated yield of 82%. NH_2-COF was reduced by $SnCl_2 \cdot 2H_2O$ using Lohse's method[2], with a yield of 88%.

Synthesis of CdS QDs.

CdS QDs were synthesized according to a standard method [3]. Typically, an aqueous solution (20 mL) containing $CdCl_2$(1 mmol) and 3-MPA (1.7 mmol) was prepared, and its pH was adjusted to 10 using a 2.0 M NaOH solution. The resulting mixture was transferred to a 50 mL three-necked

flask, which was purged with Ar to remove air. After stirring at room temperature for 30 minutes, 1 mL of Na_2S solution (containing 1 mmol of Na_2S) was rapidly injected into the flask, and the reaction temperature was set to 100 °C. After 1 hour of reaction, the system was allowed to cool naturally to room temperature. Ethanol was added to the mixture, and the product was separated by centrifugation. It was then redispersed in an aqueous solution for subsequent use.

Synthesis of NH_2-COF/CdS and NO_2-COF/CdS.

Firstly, 150 mg of NH_2-COF was ball-milled at 600 revolutions per second for 3 hours, then dispersed in 10 mL of water. The dispersion was transferred to a 50 mL three-necked flask and stirred for 2 hours (serving as the pretreated NH_2-COF). Separately, the cadmium precursor was prepared by dissolving $CdCl_2$ (0.5 mmol) and 3-MPA (0.85 mmol) in deionized water (10 mL), followed by pH adjustment to ~10 with 2.0 M NaOH. The above-prepared cadmium precursor solution was added to the three-necked flask containing the pretreated NH_2-COF, and the combined mixture's pH was readjusted to 10. The mixture was bubbled with argon (Ar) to purge air; after 30 minutes, 1 mL of sodium sulfide (Na_2S) solution (containing 0.5 mmol of Na_2S) was rapidly injected into the flask. The temperature was swiftly elevated to 100 °C and held for 1 h. The final product was recovered by centrifugation, washed repeatedly with deionized water and ethanol, and vacuum-dried at 60 °C for 12 h. The resulting composite catalyst was designated as NH_2-COF/CdS-1. By varying the dosage of the cadmium precursor solution (0.25, 1, and 2 mmol), materials with different CdS loadings were obtained, and the corresponding catalysts are designated as NH_2-COF/CdS-0.25, NH_2-COF/CdS-1, NH_2-COF/CdS-2 and NO_2-COF/CdS-0.5, respectively.

Characterization

The PXRD pattern of the samples was recorded on an X-ray diffractometer with Cu-Kα

radiation (D8 Advance, Bruker Ltd., Germany). The distribution of co-catalysts was observed by transmission electron microscopy (TEM). Porosity was measured using the BET instrument (ASAP2460, Micromeritics). Fourier transform infrared spectroscopy (FTIR) spectra were recorded on a TENSOR 27 spectrometer (Bruker Ltd., Germany). UV-Vis-DRS spectroscopy was performed using a PerkinElmer Lambda 950. The X-ray photoelectron spectra (XPS) were examined with Thermo Kalpha. The photoluminescence spectra (PL) of the samples were recorded in SPEX Fluorolog-3 spectrofluorometer. Thermogravimetric analysis (TGA) was performed on a Netzsch STA 499C instrument under nitrogen atmosphere at a heating rate of $10°C \cdot min^{-1}$ to evaluate the thermal stability of the as-prepared samples. Atomic force microscopy (AFM) images were obtained using a Bruker Dimension ICON microscope to characterize the thickness and morphology of the nanosheets. Elemental analysis (C, H, N, S) was carried out on an Elementar Vario EL III elemental analyzer to determine the composition of the COF and its composites.

Photoelectrochemical measurements

The Mott-Schottky plot (M-S), transient photocurrent spectra (I-T) and electrochemical impedance spectra (EIS) measurements were conducted on a CHI660E electrochemical workstation in a three-electrode cell system under ambient conditions under irradiation of a 300 W Xe lamp. The ITO coated photocatalyst as the working electrode, a Pt foil as the counter electrode, and an Ag/AgCl electrode as the reference electrode. The three electrodes were inserted in a beaker filled with 0.5 M Na_2SO_4 electrolyte.

Computational details

In the calculations, density functional theory (DFT) was performed with the Vienna Abinitio Simulation Package (VASP), [4] The projector augmented wave (PAW) methods were applied for the

interactions between valence electrons and atomic nucleus.[5] The electron exchange-correlation function used the Perdew-Burke-Emnzerhof (PBE) of the generalized gradient approximation (GGA). The energy cut-off of the wave function in the plane-wave basis was selected, The DFT-D2 method was used to describe the van der Waals interaction. Additionally, the K point sampling of Brillouin zone only used the gamma point of 1×1×1 Monkhorst-Pack scheme. The calculations were terminated until the maximum force upon each atom and energy were less than 0.02eV/Ã and 1.0×10-5 eV, Spin polarization was used throughout the calculation.

Evaluation of photocatalytic OWS reaction

Photocatalytic reactions for overall water splitting were conducted in a Pyrex top-irradiation reaction vessel using a Perfect Light (Labsolar 6A) closed gas circulation system. In each reaction, 5mg of the photocatalyst was dispersed in 100 mL of deionized water. 5wt% Pt was photodeposited in-situ as the hydrogen evolution cocatalyst before the photocatalytic reaction. A 300 W xenon lamp equipped with an AM 1.5G filter served as the light source, with an irradiance intensity of 100 mW cm^{-2} (standard solar intensity) covering the wavelength range of 300-1100 nm. The reaction temperature was maintained at 25°C by a circulating cooling water system throughout the experiment. The products were analyzed by online 9790 gas chromatography (Agilent) with argon (AR) as the carrier gas. Following the photocatalytic experiment, the photocatalyst was washed with water and acetone, collected, and then dried under vacuum at 60°C. The photocatalytic OWS performance of NH_2-COF/CdS was studied.

Supplementary figures and table

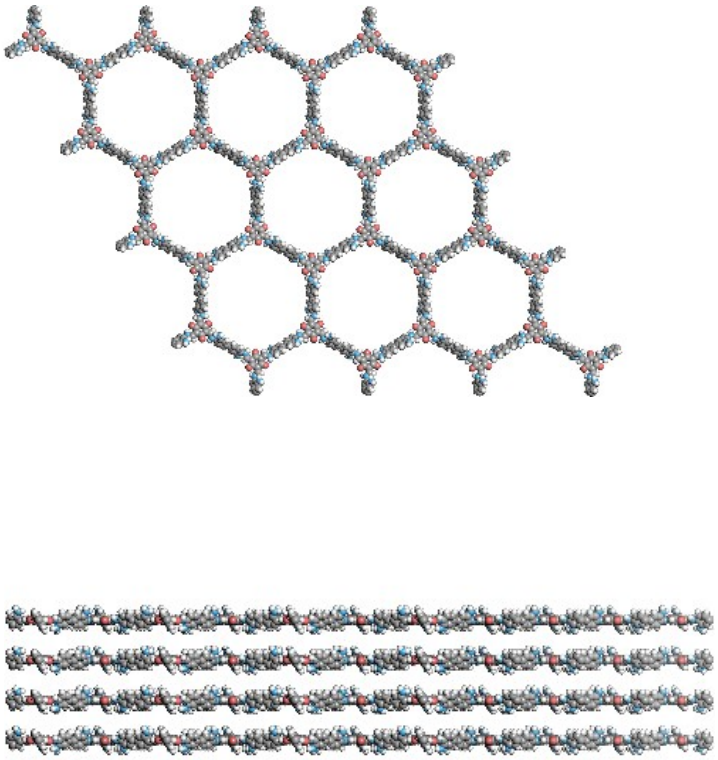

Figure S1 Chemical structure model diagram of NH_2-COF.

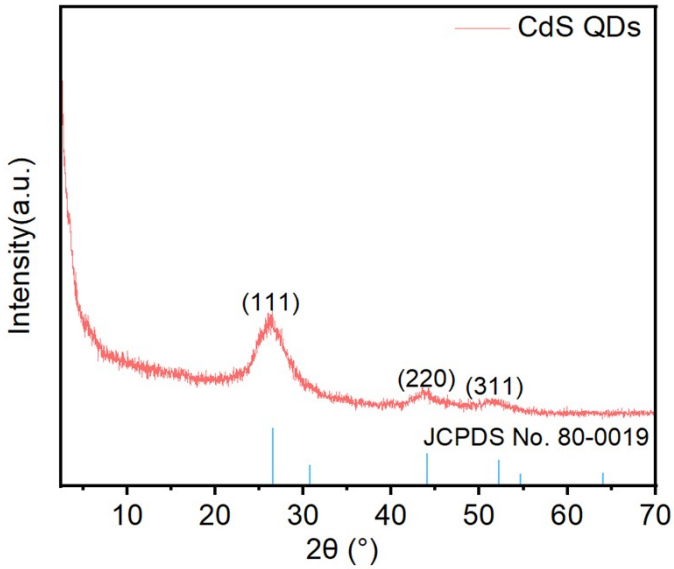

Figure S2. Experimental PXRD patterns of CdS QDs and standard card (No. 80-0019) of CdS.

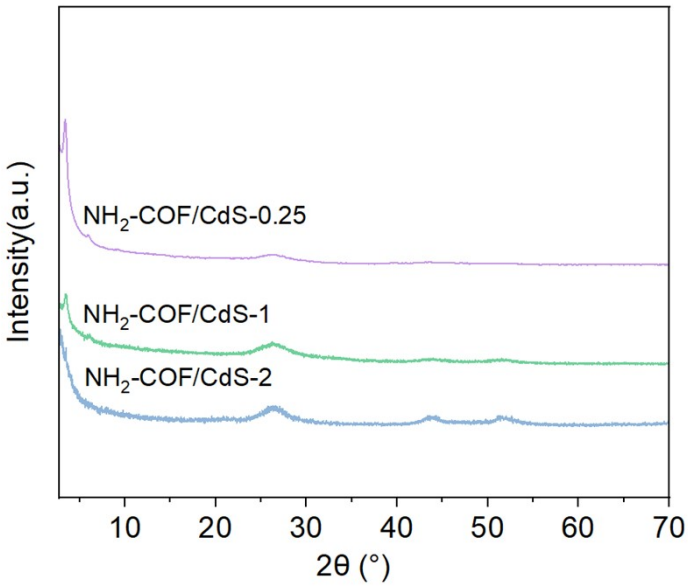

Figure S3. Experimental PXRD patterns of NH_2-COF/CdS-x (x=0.25, 1, 2).

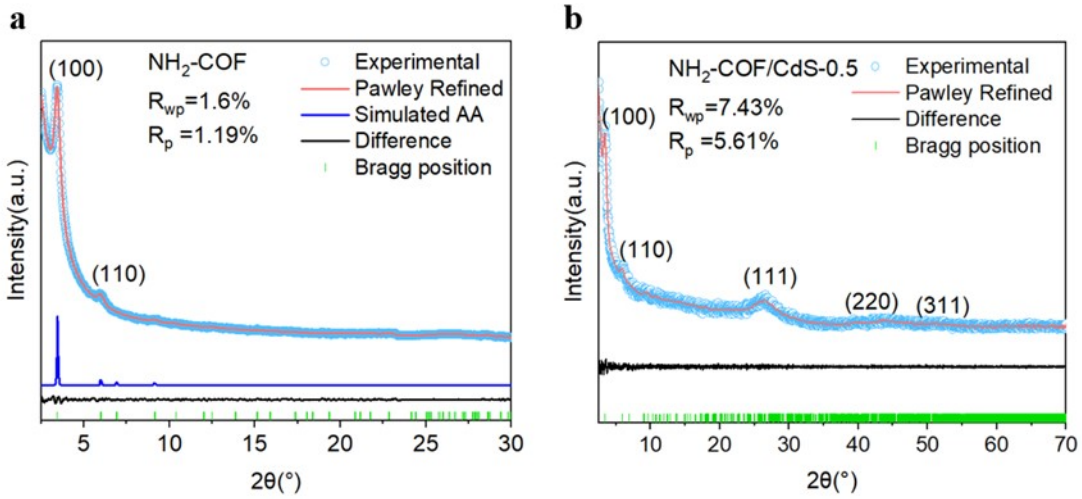

Figure S4. Pawley refinement data of (a)NH_2-COFand (b) NH_2-COF/CdS-0.5.

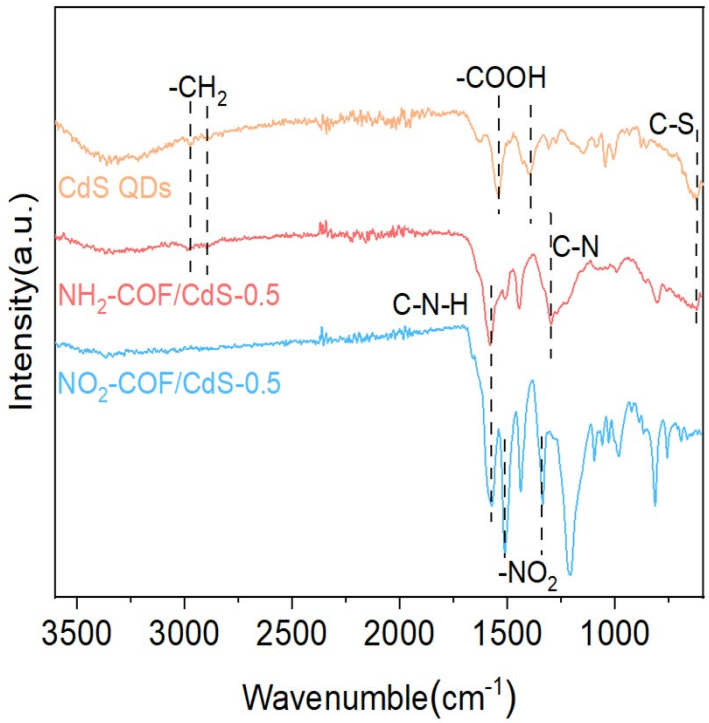

Figure S5. FTIR spectra of NO_2-COF/CdS-0.5, NH_2-COF/CdS-0.5 and CdS QDs.

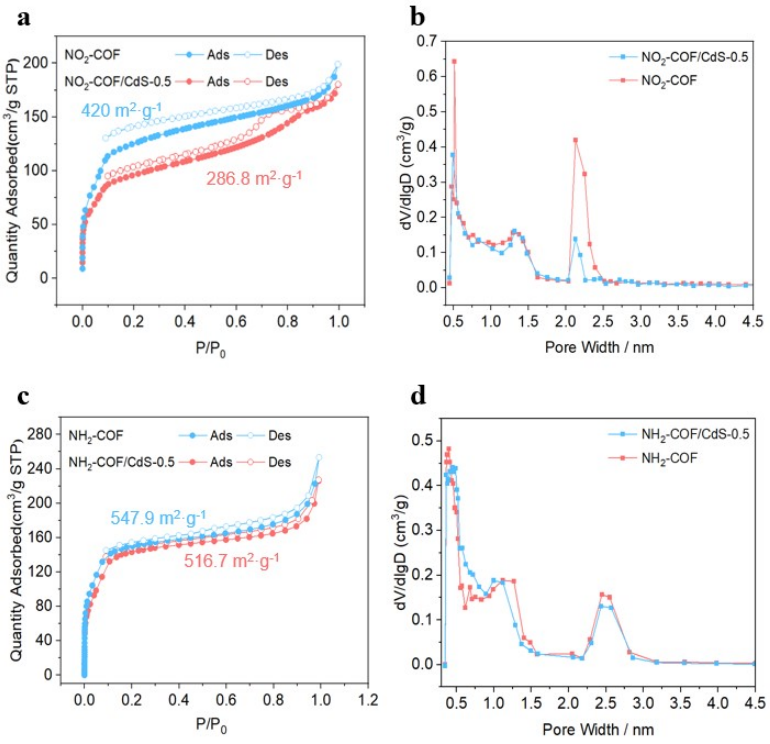

Figure S6. N_2 adsorption-desorption measurements and Pore size distributions of NO_2-COF, NO_2-COF/CdS-0.5, NH_2-COF, and the NH_2-COF/CdS-0.5.

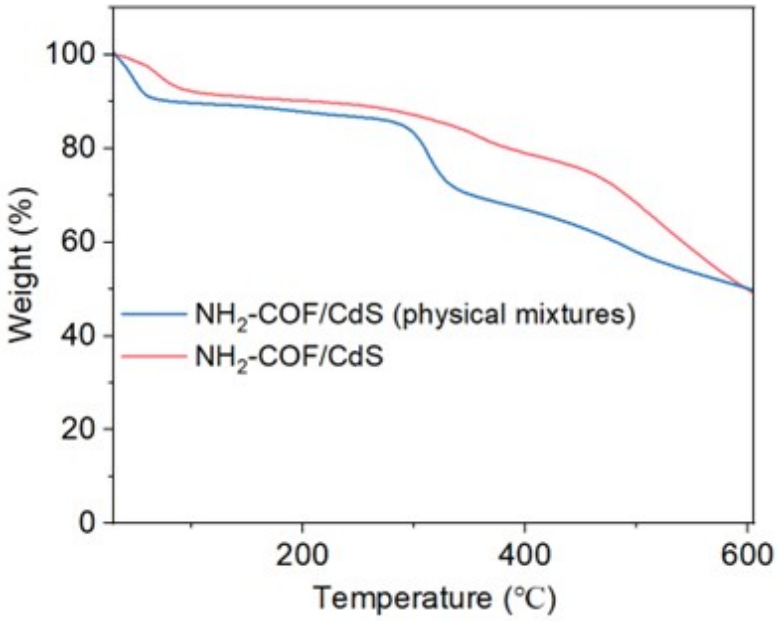

Figure S7. TGA spectra of physically mixed NH_2-COF/CdS and NH_2-COF/CdS composites.

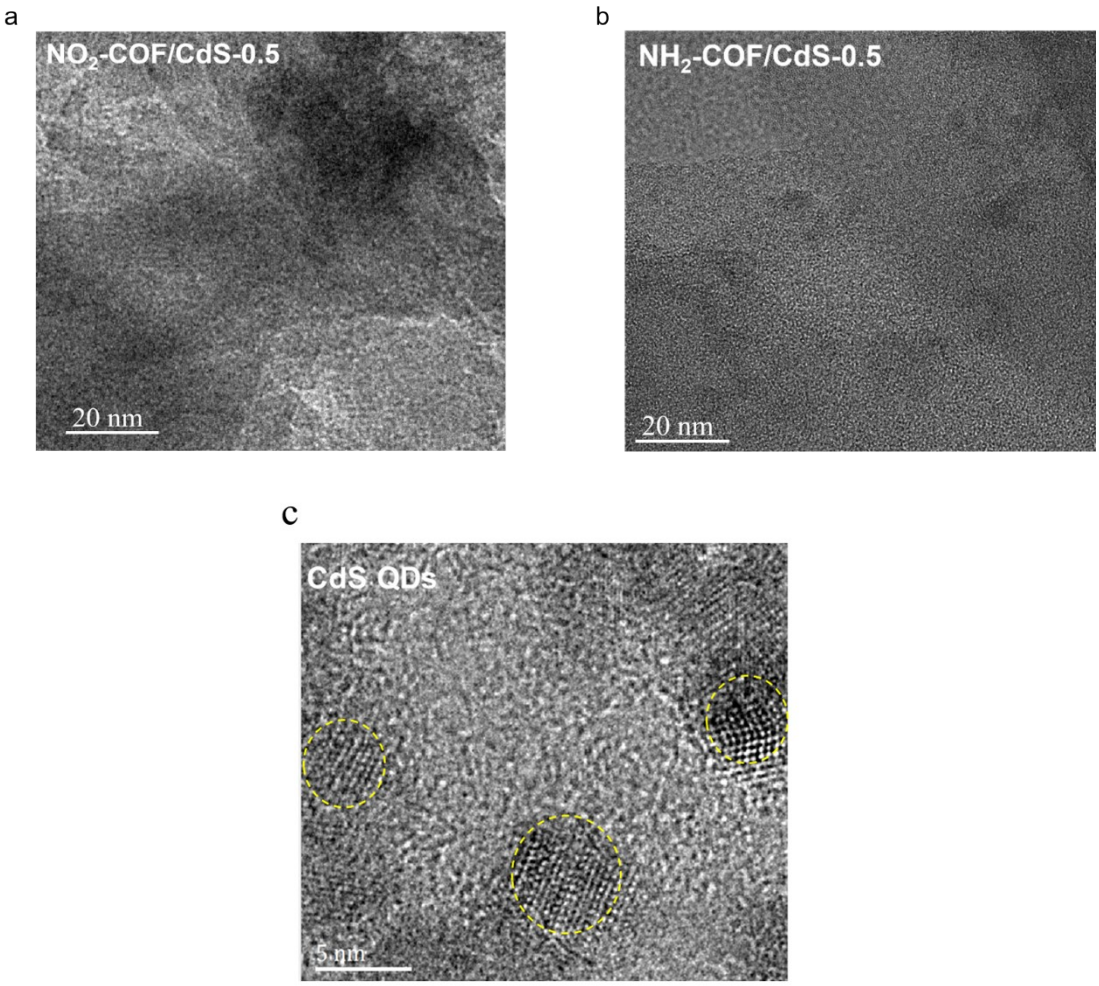

Figure S8. TEM of (a) NO_2-COF/CdS-0.5, (b) NH_2-COF/CdS-0.5 and (c) CdS QDs.

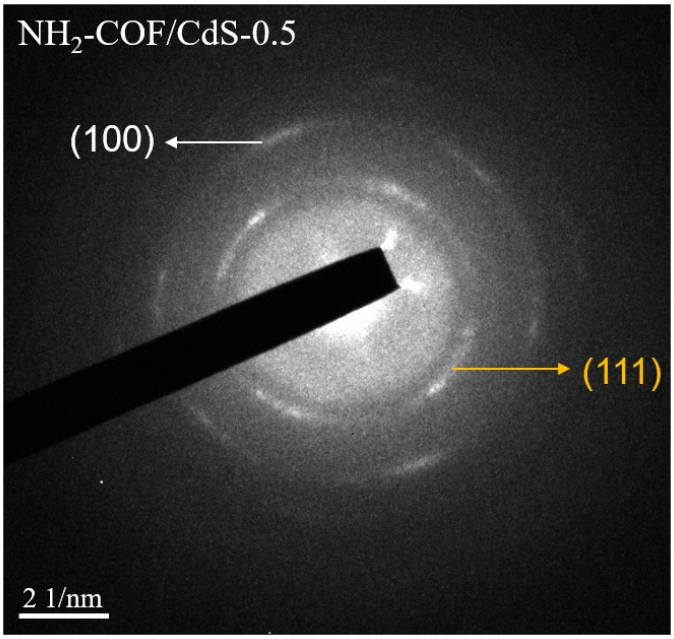

Figure S9. SAED pattern of NH_2-COF/CdS-0.5.

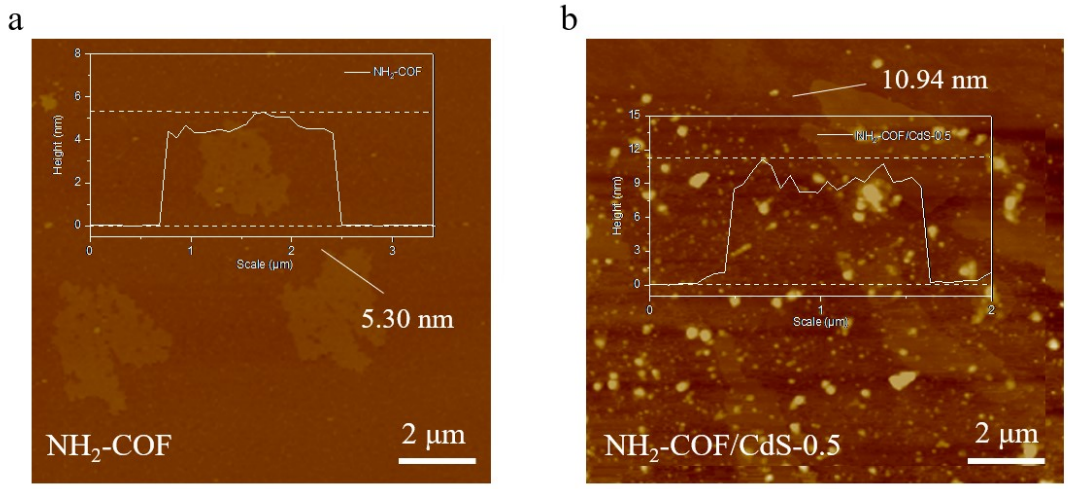

Figure S10. Atomic force microscopy (AFM) images and corresponding height profiles of (a) NH_2-COF and (b) NH_2-COF/CdS-0.5 composite.

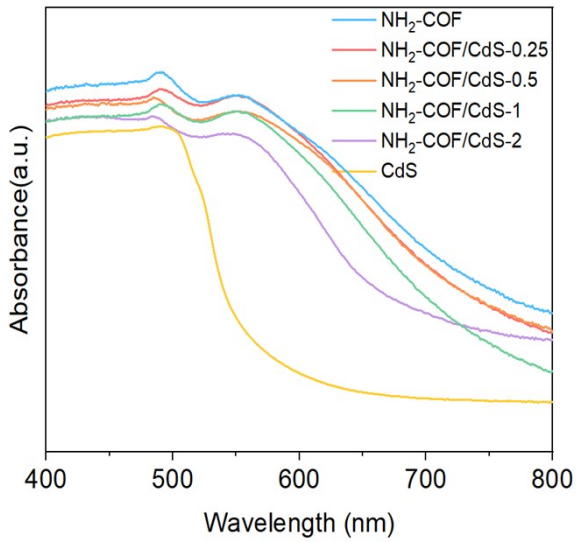

Figure S11. UV-vis DRS spectra of NH_2-COF, CdS, and composite.

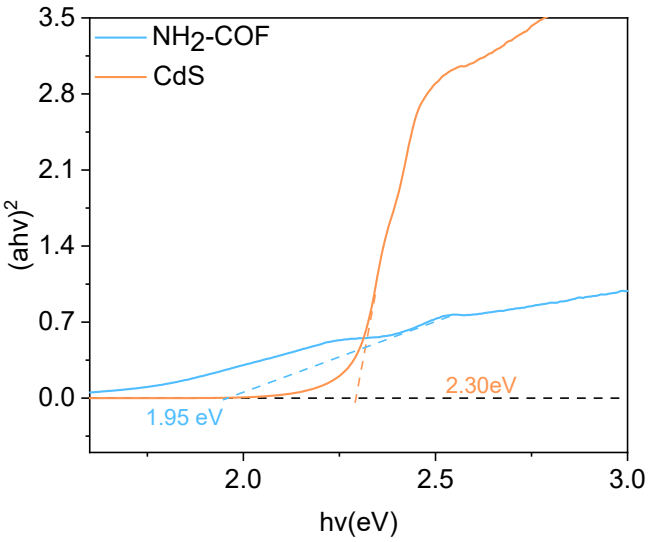

Figure S12. Tauc Plots of NH_2-COF and CdS QDs.

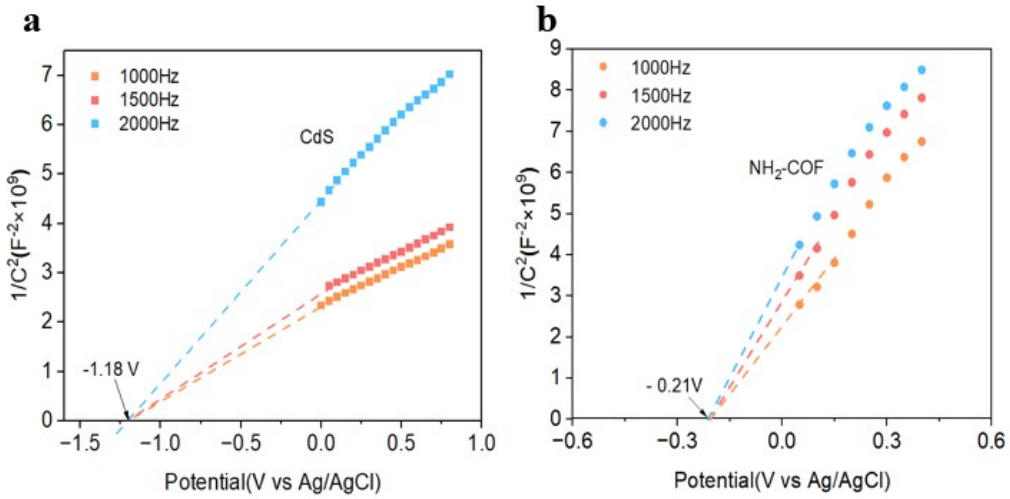

Figure S13. Mott-Schottky plots of CdS QDs (a) and NH_2-COF (b). The flat band potentials were obtained from the Mott-Schottky plots. Both NH_2-COF and CdS QDs exhibit n-type semiconductor characteristics, with flat band potentials of -0.21 V (vs Ag/AgCl) for NH_2-COF and -1.18 V vs (Ag/AgCl) for CdS QDs. These values correspond to conduction band (CB) positions of -0.01 V and -0.98 V (vs. NHE, pH = 7). Subsequent calculation of the valence band (VB) positions, leveraging the optical band gaps, yielded values of +1.94 V for NH_2-COF and +1.32 V for CdS.

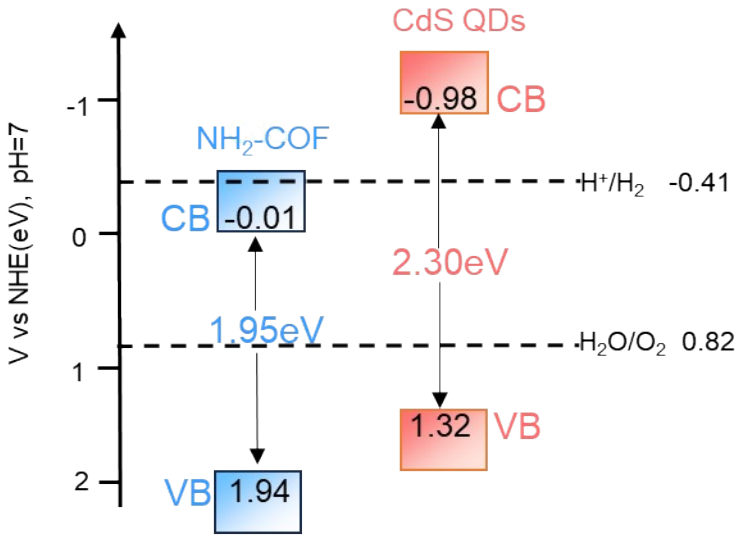

Figure S14. Band structure diagram of NH_2-COF and CdS QDs.

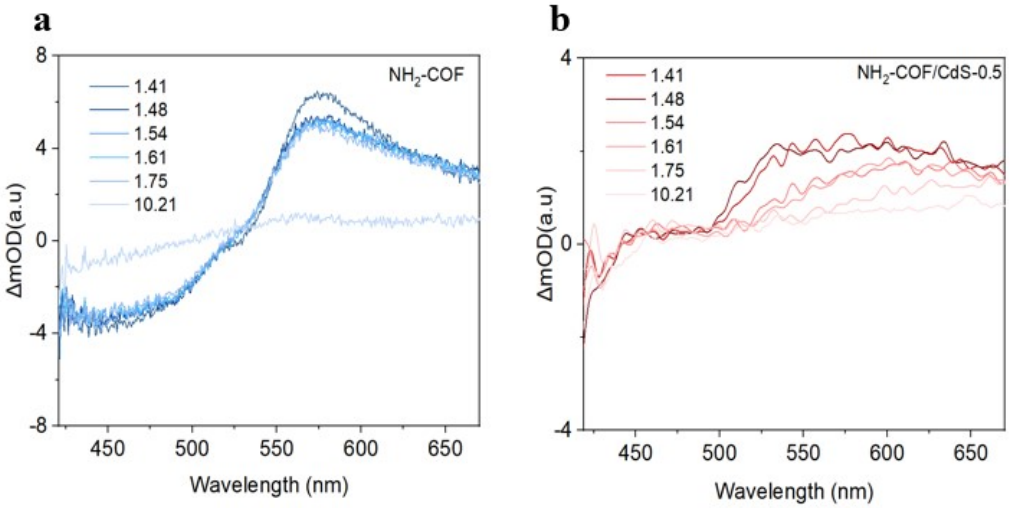

Figure S15. TA plots recorded at the indicated delay time for (a) NH_2-COF and (b)NH_2-COF/CdS-0.5.

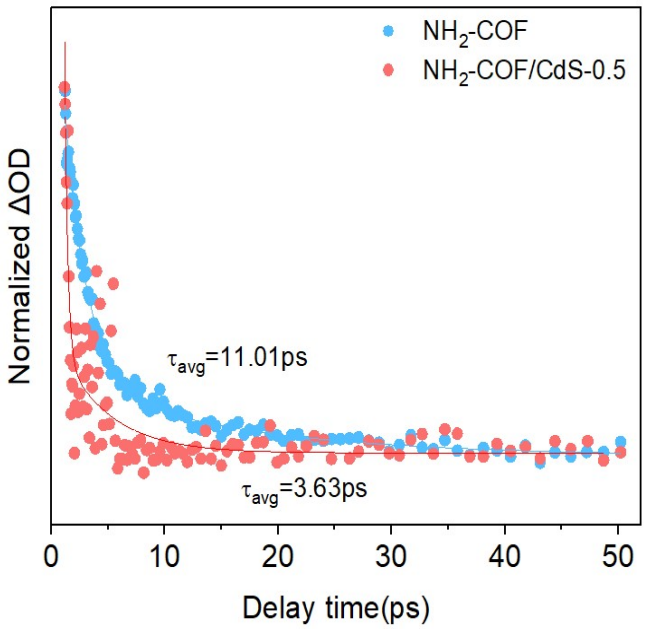

Figure S16. Normalized decay kinetic curves of NH_2-COF and NH_2-COF/CdS-0.5 at 574 nm.

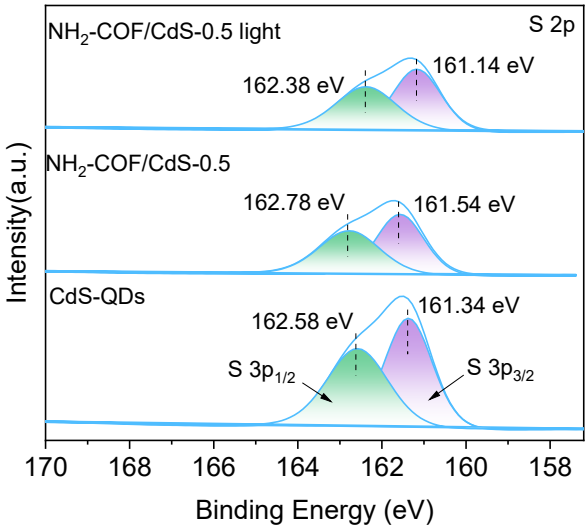

Figure S17. High-resolution XPS spectra of S 2p for NH_2-COF/CdS-0.5.

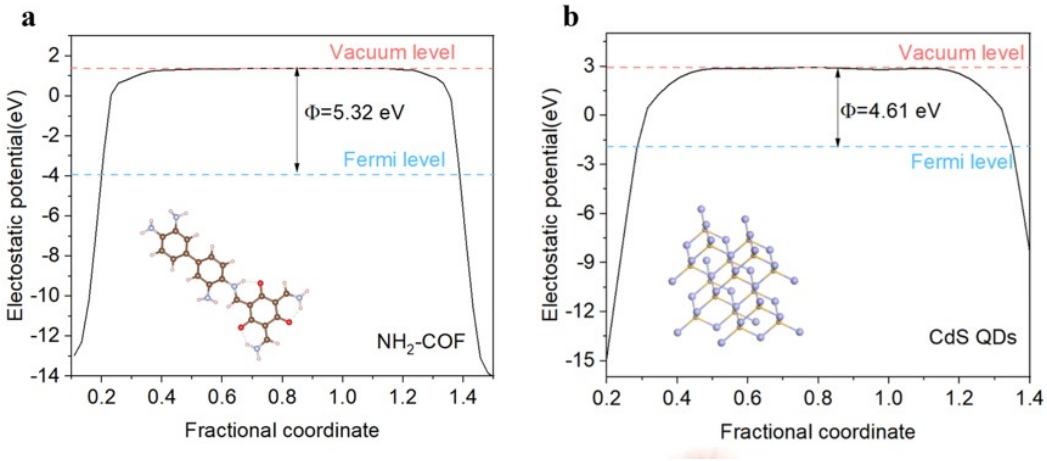

Figure S18. DFT-calculated work functions of (a) NH_2-COF and (b) CdS QDs.

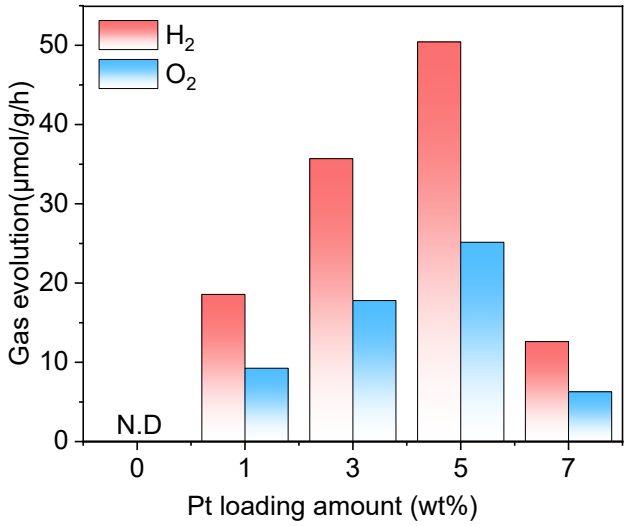

Figure S19. The photocatalytic OWS activities over Pt (X wt%) NH_2-COF/CdS-1. (X=0 ,1 ,3 ,5 ,7 wt%)

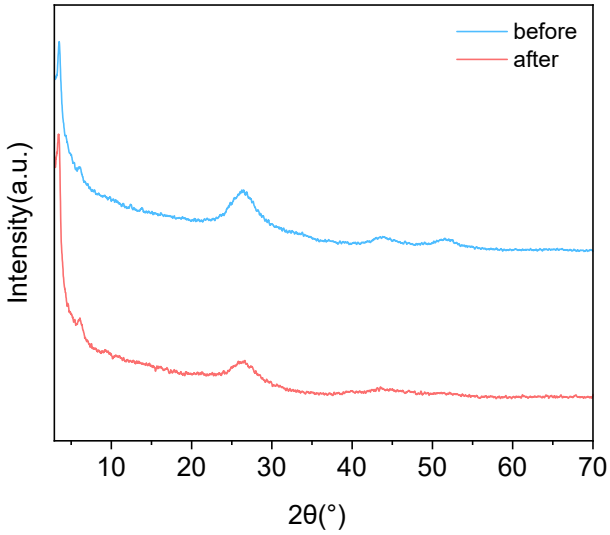

Figure S20. The PXRD patterns of NH_2-COF/CdS-0.5 composites before and after photocatalysis reaction.

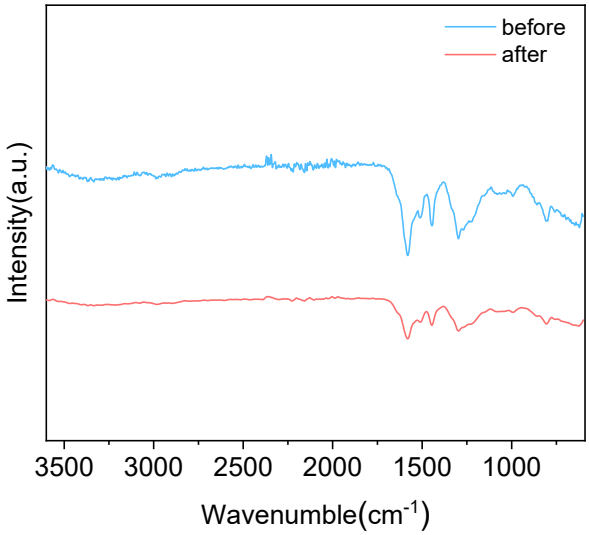

Figure S21.The FT-IR spectra of NH_2-COF/CdS-0.5 composites before and after photocatalysis reaction.

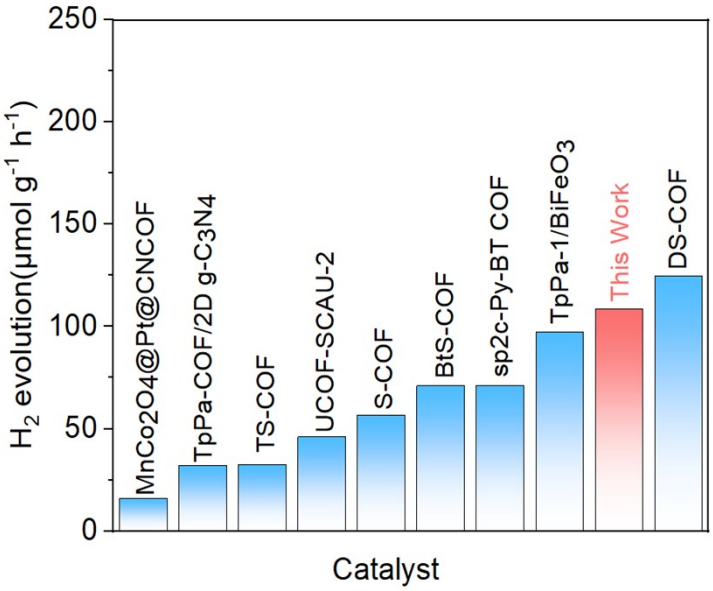

Figure S22.Comparison of catalytic overall water splitting rate of COFs and COFs-based photocatalysts.

Table S1. CHNS elemental analysis results of COFs and COFs/CdS-0.5.

COF[a]	C (wt%)	H (wt%)	N (wt%)	S (wt%)
	Expt.	Expt.	Expt.	Expt.
NO_2-COF	56.41	2.85	14.39	0
NH_2-COF	66.65	4.91	17.02	0
NO_2-COF/CdS-0.5	51.23	2.45	12.89	1.56
NH_2-COF/CdS-0.5	60.15	4.04	15.72	4.32

[a] Expt. = experimental value.

Table S2. The comparison of the photocatalytic OWS on COF and COF-based photocatalysts.

Photocatalysts	Cocatalyst	HER ($\mu mol\ g^{-1}\ h^{-1}$)	OER ($\mu mol\ g^{-1}\ h^{-1}$)	Ref.
NH_2-COF/CdS-0.5	Pt	108.7	52.2	This work
$MnCo_2O_4$@Pt@CNCOF	Ag@Cr_2O_3	16.2	7.8	6
TpPa-COF/2D g-C_3N_4	Ag@Cr_2O_3 Pt	32	15.8	7
TS-COF	Pt IrO_2	32.5	16.3	8
UCOF-SCAU-2	Pt	46	21	9
S-COF	Pt IrO_2	56.6	29.2	8
BtS-COF	Pt	71	34	10
sp^2c-Py-BT COF	Pt $Co(OH)_2$	71.3	30.8	11
α-Fe_2O_3/TpPa-1-COF/FeP-PC	α-Fe_2O_3 FeP-PC	97.45	48.46	12
DS-COF	Pt, IrO_2	124.7	59.4	8
0.5-γ-Ga_2O_3/CdS	/	131.7	61.8	13

BiVO4/Au/CdS	/	281	138	14
2.0%MoS_2-0.2CdS/WO_3- 1.0%MnO_2	/	633	200	15

Table S3. Comparison of COF/CdS-based photocatalysts.

Synthesis Strategy	photocatalyst	application	performance	Ref.
in-situ formation	CdS/BUCT-COF-20	photocatalytic hydrogen evolution	H_2 production rate: 1040 μmol·g^{-1}·h^{-1}	16
	PyTdCdS5	Coupled photocatalytic hydrogen peroxide generation and selective oxidation of PXG	H_2O_2 production rate: 7.86 mmol·g^{-1} PXG conversion rate: 95%	17
electrostatic self-assembly	CdS-1%COF	photocatalytic hydrogen evolution	H_2 production rate: 15.1 mmol·g^{-1} h^{-1}	18
	TFPD/CdS-2:8	photocatalytic hydrogen evolution Selective oxidation of HMF into DFF	H_2 production rate: 228.7 μmol·g^{-1}·h^{-1} HMF conversion and DFF selectivity: 91%	19
physical mixing	1.5wt%COF/CdS	photocatalytic hydrogen evolution	H_2 production rate: 8670 μmol·g^{-1} h^{-1}	20
ultrasonic-assisted method	0.5wt%CdS/COF	Visible-light photocatalytic degradation of organic pollutants	BPA removal rate after 3 h irradiation: 85.68%	21

interfacial bridging	NH_2-COF/CdS-0.5	Sacrificial-agent-free overall photocatalytic water splitting	H_2 production rate: 108.7μmol g^{-1} h^{-1} O_2 production rate: 52.2μmol g^{-1} h^{-1}	This Work

Supplementary References

1 X. Zhong, Q. Ling, P. Kuang and B. Hu, *Chemical Engineering Journal*, 2024, **483**, 149339.

2 M. S. Lohse, T. Stassin, G. Naudin, S. Wuttke, R. Ameloot, D. De Vos, D. D. Medina and T. Bein, *Chemistry of Materials*, 2016, **28**, 626-631.

3 J. Wang, T. Xia, L. Wang, X. Zheng, Z. Qi, C. Gao, J. Zhu, Z. Li, H. Xu and Y. Xiong, *Angewandte Chemie International Edition*, 2018, **57**, 16447-16451.

4 G. Kresse and J. Furthmüller, *Physical Review B*, 1996, **54**, 11169-11186.

5 J. P. Perdew, K. Burke and M. Ernzerhof, *Physical Review Letters*, 1996, **77**, 3865-3868.

6 Y. Yuan, Q. Yang, X. Li, Y. Shama, H. Yan and C. Wang, *Int. J. Hydrogen Energy*, 2024, **61**, 407-414.

7 Y. Li, J. Wang, S. Xu, M. Li and F. Chen, *Int. J. Hydrogen Energy*, 2024, **60**, 1433-1441.

8 X. Zhang, Z. Xiao, L. Jiao, H. Wu, Y.-X. Tan, J. Lin, D. Yuan and Y. Wang, *Angew. Chem. Int. Ed.*, 2024, **63**, e202408697.

9 R. Shen, C. Qin, L. Hao, X. Li, P. Zhang and X. Li, *Adv. Mater.*, 2023, **35**, 2305397.

10 Q. Niu, W. Deng, Y. Chen, Q. Lin, L. Li, Z. Liu, J. Bi and Y. Yu, *ACS Energy Lett.*, 2024, **9**, 5830-5835.

11 J. Cheng, Y. Wu, W. Zhang, J. Zhang, L. Wang, M. Zhou, F. Fan, X. Wu and H. Xu, *Adv. Mater.*, 2024, **36**, 2305313.

12 M.-L. Xu, J.-R. Li, X.-M. Wu, T. Yu, G.-Y. Qin, F.-J. Wang, L.-N. Zhang, K. Li and X. Cheng, *Appl. Surf. Sci.*, 2022, **602**, 154371.

13 X. Pan, X. Wang, Z. Zhang, C. Ma, J. Chen, Y. Yuan, H. Li, *J. Alloy. Compd.*, 2025, **1013**, 178595.

14 X. Xu, Z. Wang, W. Qiao, F. Luo, J. Hu, D. Wang, Y. Zhou, *Int. J. Hydrogen Energy.*, 2021, **46**, 8531.

15 D. Wei, Y. Ding, Z. Li, *Int. J. Hydrogen Energy.*, 2020, **45**, 17320. T. Wang, B. Yang, Z. Zhou, Y. Wu, Z. Jin, *Small*, 2025, **21**, 2501128.

16 T. Wang, B. Yang, Z. Zhou, Y. Wu, Z. Jin, *Small*, 2025, **21**, 2501128.

17 G. Tang, J. Zhang, C. Bie, X. Zheng, C. Jiang, J. Yu, *Adv. Mater.*, 2025, **37**, e14576.

18 G. Sun, J. Zhang, B. Cheng, H. Yu, J. Yu, J. Xu, *Chem. Eng. J.*, 2023, **476**, 146818.

19 B. Qi, R. Shen, Z. Ren, Y. Teng, H. Ding, X. Zhang, Y. Zhang, L. Hao, X. Li, *J. Mater. Sci. Technol.*, 2025, **232**, 65.

20 L. Sun, L. Li, J. Yang, J. Fan, Q. Xu, *Chin. J. Catal.*, 2022, **43**, 350.

21 C. Sun, L. Karuppasamy, L. Gurusamy, H.-J. Yang, C.-H. Liu, J. Dong, J. J. Wu, *Sep. Purif. Technol.*, 2021, **271**, 118873.